SOI Thin Microdosimeter Detectors for Low Energy Ions and Radiation Damage Studies

Benjamin James, Linh T. Tran, James Vohradsky, David Bolst, Vladimir Pan, Madeline Carr, Susanna Guatelli, Alex Pogossov, Marco Petasecca, Michael Lerch, Dale A. Prokopovich, Mark I. Reinhard, Marco Povoli, Angela Kok, David Hinde, Mahananda Dasgupta, Andrew Stuchbery, Vladimir Perevertaylo and Anatoly B. Rosenfeld

***Abstract* - The responses of two silicon on insulator (SOI) 3D microdosimeters developed by the Centre for Medical Radiation Physics (CMRP) were investigated with a range of different low energy ions, with high linear energy transfer (LET). The two microdosimeters n-SOI and p-SOI were able to measure the LET of different ions including ^{7}Li, ^{12}C, ^{16}O and ^{48}Ti with ranges below 350 µm in silicon. No plasma effects were seen in the SOI microdosimeters when irradiated with the high LET ions. A Monte Carlo simulation using Geant4 was compared to the experimental measurements, whereby some discrepancies were observed for heavier ions at lower energies. This discrepancy can be partly attributed to uncertainties in the thickness of the energy degraders and overlayers of the devices. The microdosimetric measurements of low energy ^{16}O ions were obtained and compared to a therapeutic ^{16}O ion beam. The radiation hardness of the two devices was studied using the Ion Beam Induced Charge Collection technique (IBIC). Both types of microdosimeters when biased had no essential changes in charge collection efficiency (CCE) in the SV after irradiation with low energy ions.**

I. Introduction

In deep space environments where high energy heavy ions are observed, their linear energy transfer (LET) spectrum is important to be characterized and monitored due to their adverse effects on human health as well as electronic components. This becomes especially important within the interior of the spacecraft. After passing through shielding materials, the energy of the incident ions can be sufficiently reduced. Additionally, secondary particles with greatly reduced energy can be produced. These lower energy ions can have very high LET, which can cause biological damage when passing through the body of astronauts and cause radiation damage in electronic components. The aim of this work was to study the applicability of silicon microdosimeters for high LET ion measurements.

This study was performed using two different silicon on insulator (SOI) microdosimeter designs, with one being an n-type and the other a p-type device. The radiation hardness of these two designs was investigated with respect to being irradiated by different high LET ions.

The SOI microdosimeters have the advantage of simpler operation and compact size compared to conventional tissue equivalent proportional counters (TEPC) [1]. In addition to radiation protection in space, the high spatial resolution silicon microdosimeters are desirable in hadron therapy since they allow detailed characterization of the beam at the distal part of the Bragg peak (BP) where energy of ions is low and their LET is high. Currently, ions such as Carbon, Oxygen and Lithium are being used and investigated in clinical scenarios to perform heavy ion therapy [2]. The effect of these low energy primary ions at the distal part of the BP is masked by the extensive secondary radiation field generated which includes fragments and neutrons produced within the target. This work examines the characteristics of a highly pure low energy ion beam in the absence of most secondary particles and range straggling of the ion beam, contrasting to ion beams typical of hadron therapy.

Microdosimetry is a convenient method to obtain the dose equivalent of any mixed radiation field. This is particularly important for ions since they produce a complex radiation field made up of many different secondary fragments, neutrons, photons and electrons with a large range of LET. Regional microdosimetry is based on the measurement of ionizing energy deposited in a micron sized volume of similar dimensions to biological cells. The energy deposition event by event spectrum in such a volume is called the lineal energy deposition$(y) := E/< l >$, where E is the energy deposited in a micron sized sensitive volume (SV) with a mean chord length $< l >$ and the spectrum of stochastic events $f(y)$ for all primary and secondary charged particles.

II. Method

This work involved using two SOI microdosimeters to make LET measurements in silicon for low energy ions with ranges of less than a few hundred µm in silicon. The microdosimetric quantity, the dose mean lineal energy $\overline{y_D}$, was also calculated and compared to an ^{16}O therapeutic ion beam.

This paper was originally submitted for review on 13/07/2018, with resubmission for revision on 22/10/2018. This research was supported by the Australian Government through the Australian Research Council's Discovery Projects funding scheme (projects DP 170102273 and DP170102423).

B. James, L. T. Tran, J. Vohradsky, D. Bolst, V. Pan, M. Carr, S. Guatelli, A. Pogossov, M. Petasecca, M. Lerch and A. B. Rosenfeld are with the Centre for Medical Radiation Physics, University of Wollongong, NSW, 2522, Australia (email: bj197@uowmail.edu.au; tltran@uow.edu.au; jev720@uowmail.edu.au; db001@uowmail.edu.au; vp881@uowmail.edu.au; mec640@uowmail.edu.au; susanna@uow.edu.au; apogosso@tpg.com.au; marcop@uow.edu.au; mlerch@uow.edu.au; anatoly@uow.edu.au).

D. A. Prokopovich and M. I. Reinhard are with the NSTLI Nuclear Stewardship Platform, Australian Nuclear Science and Technology Organisation (ANSTO), Lucas Heights, NSW 2234, Australia (email: dale.prokopovich@ansto.gov.au; mark.reinhard@ansto.gov.au)

M. Povoli and A. Kok are with SINTEF, Norway (email: marco.povoli@sintef.no; angela.kok@sintef.no)

D. Hinde, M. Dasgupta and A. Stuchbery are with the Department of Nuclear Physics, Australian National University, Canberra, Australia (email: david.hinde@anu.edu.au; mahananda.dasgupta@anu.edu.au; andrew.stuchbery@anu.edu.au)

V. Perevertaylo is with SPA-BIT, Ukraine (email: detector@carrier.kiev.ua)

A. *Detector Structures*

The two detectors used in this work are called the Bridge and the Mushroom. The Bridge microdosimeter has a total sensitive area of 4.1 x 3.6 mm^2 and is segmented into three sections to reduce the noise by minimizing the capacitance and reverse current of each segment. The microdosimeter is based on an array of planar 30 x 30 x 10 µm cubic SVs fabricated on a high resistivity of 3 kΩ.cm n-SOI active layer of thickness 10 µm and low resistivity supporting wafer [4]. Fig. 1 presents SEM images showing arrays of the Bridge's SVs.

The Mushroom microdosimeter structure used in this work is called a trenched 3D and it consists of 3D cylindrical SVs with a core columnar n+ and each SV is surrounded with p+ trench to form a p-n junction. The Mushroom microdosimeter has a thickness of 9.1 um and diameter of 30 µm fabricated on high resistivity p-type silicon (> 10 kΩ.cm). Each SV is surrounded with a trench of air with p^+ doping on the outer wall, designed to physically eliminate the possibility of charge generated outside the SV from being collected. In order to electrically connect SVs in an array, two half-moon trenches were made by leaving some silicon present for the metal contacts between the inner n^+ electrodes. Outer Al buses were connected to p^+ outer electrodes of 3D SVs [3]. Fig. 2 shows SEM images of arrays of Mushroom SVs (a) and a single SV (b).

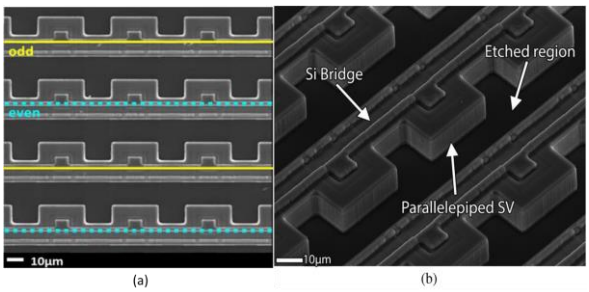

Fig. 1. SEM images of arrays of Bridge SVs. (a) Array of SVs. (b) Arrays of SVs tilted at 45° [4]

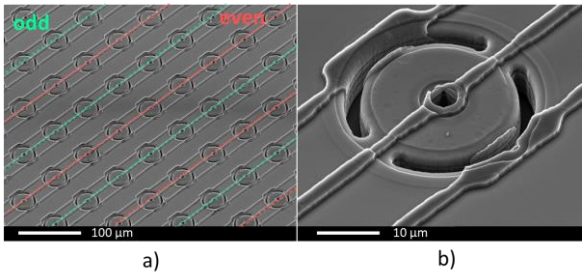

Fig. 2. SEM images of 3D Mushroom microdosimeter SVs. (a) Array of SVs. (b) Single SV [3]

Both detectors utilise the fact that even and odd rows of SVs are read out independently to avoid events in adjacent sensitive volumes being read as a single event in the case of oblique charged particle tracks. The charge collection and response of these detectors has been thoroughly investigated and documented in previous works [3], [4].

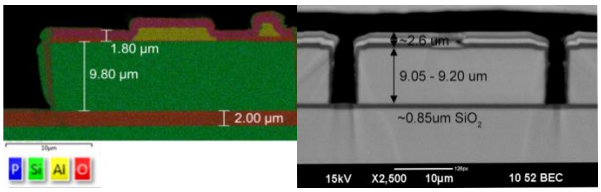

Fig. 3. Scanning electron microscope cross section images of a) Bridge and b) Mushroom microdosimeter

Fig. 3 shows SEM images of the cross sections of the Bridge (a) and Mushroom (b) microdosimeters and shows the overlayer structures of the devices. The uniformity of these overlayer structure thicknesses can affect the accuracy of estimating the entrance ion energy reaching the SV. The uncertainty of the ion energy when it reaches the SV, increases as the LET of the ion increases. With maximum values of LET reaching ~6000 keV/µm for Ti, the uncertainty of ion energy could be high

B. *Low Energy Ion Irradiation*

The Heavy Ion Accelerator Facility (HIAF) comprises the 14UD pelletron accelerator and a superconducting 'booster' linear accelerator (LINAC) housed and operated by the Department of Nuclear Physics in the Research School of Physics and Engineering at the Australian National University. Using the 14UD pelletron accelerator, four ion species were accelerated with a fractional energy spread of less than 4 x 10^{-4}. Table I shows a list of ion species with their energy and range in silicon calculated using SRIM [5].

Using a specially generated low intensity beam (beam fluence of approximately 1200 particles/s), irradiations were conducted using both the Bridge and Mushroom 3D microdosimeters.

Ion Species	Energy (MeV)	Range in Si (µm)	LET(Si) at max energy (keV/µm)	Max LET(Si) (keV/µm)
Li-7	52	331	92	525
C-12	70	103	444	1190
O-16	118	121	643	1663
Ti-48	170	35	5061	5627

Table I. Table of ion species with their energy and range in silicon

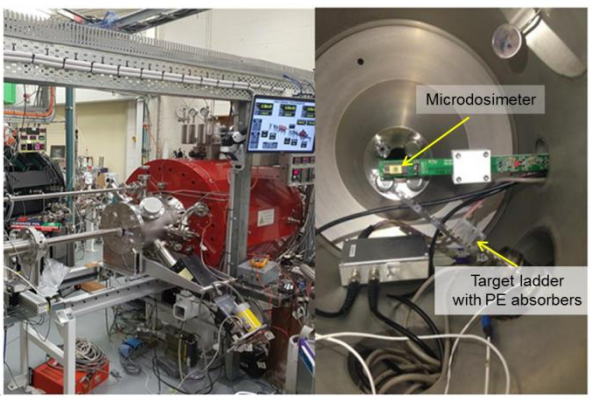

Fig. 4. ANU Experimental setup, showing both external (left) and internal (right) view of the vacuum chamber.

Both the 3D Mushroom and Bridge microdosimeter were connected to a low noise spectroscopy-based readout circuit, allowing lineal energy measurements as low as 0.15 keV/µm in tissue [3]. The shaping amplifier was set on low gain to allow the probe to measure up to approximately 15 MeV energy range for Li, C and O ions. For Ti ions, due to their high LET, the required dynamic range needed to be increased up to 80 MeV. Therefore, the charge sensitivity of the charge sensitive preamplifier was further reduced by increasing the value of the feedback capacitor.

The probe was placed in a fixed position within the vacuum chamber, shown in Fig. 4 and differing thicknesses of low density polyethylene (LDPE 0.92g/cm^3) were loaded into the target ladder, which intersects the beam path to the detector, allowing for differing positions along the Bragg curve to be measured. The thicknesses of the LDPE films were measured using a micrometer with an uncertainty of ± 2 µm. Different combinations of LDPE thicknesses were attached to Al frames which were mounted onto the movable target ladder inside the vacuum chamber. Using the target ladder allows different film thicknesses to be loaded in front of the detector without opening the vacuum chamber.

C. *LET Calculations for Low Energy Ions Using Geant4 and SRIM*

Since the maximum energy of delta electrons for ions used in this study is less than 10 keV which correspond to ranges of less than 8 µm in silicon [6], the majority of delta electrons are contained within the SV region of the microdosimeter and the measured energy deposited closely represents the total energy lost by the ion in silicon. We define the quantity LET_{MCA}, calculated for the experiment and Geant4 simulation. This differs from the LET provided by SRIM which is the theoretical energy lost by the ion in silicon. LET_{MCA} is defined as the peak of the highest energy obtained in the multichannel analyser (MCA) spectrum divided by the SOI active layer thickness of the microdosimeter. The ion energy for each experimentally obtained LET_{MCA} value corresponds to the energy of the ion after traversing polyethylene energy absorber as calculated using SRIM. Similarly, the same kinetic energy of the ions was used as an input for Geant4 calculations. The thicknesses of the active SOI layer Bridge microdosimeter and Mushroom microdosimeter are 9.8 µm and 9.1 µm, respectively (measured using SEM).

D. *Geant4 Modeling*

A dedicated Geant4 (version 10.01) simulation application [7], [8] was developed for this study to calculate the energy deposition distributions deriving from the incident ion beam within the silicon sensitive volumes of the detectors.

The Geant4 Low Energy Physics Package, based on Livermore data libraries was selected to describe the electromagnetic interactions of particles. The threshold of production for e-, e+ and ɣ was set to 250 eV, which is the lower limit of validity of this physics model [9], [10]. The Geant4 QGSP BIC HP (high-precision) physics list was selected to model the hadronic physics processes.

In order to model interactions taking place within the target sensitive volume, both the Bridge and Mushroom microdosimeter were accurately modelled within the Geant4 simulation. The simulation occurs in a vacuum with the primary beam generated 50.5 mm from the top of the detector with a circular shape 5 mm diameter.

E. *Charge Collection Study – Radiation Damage*

Radiation damage of the Bridge and Mushroom microdosimeters was studied using the ion beam induced charge collection technique (IBIC) at the 6 MV accelerator SIRIUS, located at the Centre for Accelerator Science (CAS) facility at ANSTO. This system includes a Confocal Heavy Ion Micro-Probe (CHIMP) which is capable of delivering Carbon, Helium and Hydrogen ions with energies of 24 MeV, 5.5 MeV and 8 MeV, respectively. This beamline is widely used for analysing and characterising samples using ion beam analysis (IBA) and produces high-current and high brightness ion beams with exceptional energy resolution [11].

The IBIC measurements utilized a microbeam of 5.5 MeV He^{2+} ions and 24 MeV $Carbon^{6+}$ ions which were raster scanned over the surface of the sample. The spot size of the microbeam is approximately 1 µm. Energy deposited in the microdosimeter was measured using an AMPTEK A250 charge sensitive preamplifier and a Canberra 2025 Shaping Amplifier with 1 µs shaping time. The signal corresponding to the beam's position as well as the charge collection for each event was processed into an event-by-event list mode file. The data was processed into median charge collection image maps for spatial correlation of the energy deposition of the scanned area [3] The energy calibration was performed using a calibrated pulse generator which was calibrated with a 300 µm thick planar silicon fully depleted Hamamatsu PIN photodiode with 100% Charge Collection Efficiency (CCE) in response to 5.5 MeV He^{2+} and 24 MeV C^{6+} ions.

F. *Energy Calibration for the Microdosimeters*

The energy calibration for a Mushroom microdosimeter was performed using a calibrated pulse generator which was calibrated with a planar silicon Hamamatsu PIN diode in response to a 5.486 MeV ^{241}Am source. The energy calibration for a Bridge microdosimeter was performed using 3.183 MeV alphas from a ^{148}Gd source which fully stop within the SV. The calibrated pulse generator was then used to generate different energy peaks for calibration.

III. Results and Discussion

A. *LET Study of Low Energy Ions*

Fig. 5 shows MCA spectra obtained with the Bridge and Mushroom microdosimeter in response to 70 MeV ^{12}C ions with 90 µm of polyethylene before the detectors. The deposited energy was found by selecting the peak of the highest energy for the Bridge and Mushroom microdosimeters. Due to the more complicated structure of overlayers on the Bridge microdosimeter compared to the Mushroom, the MCA spectrum of the Bridge shows multiple energy peaks for the low energy ions (high LET).

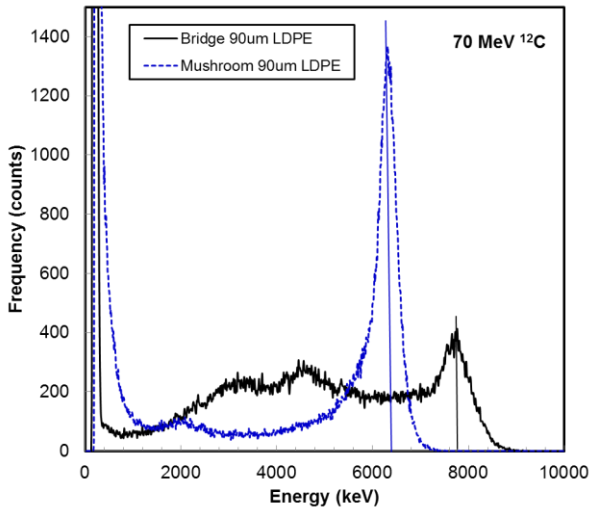

Fig. 5. MCA spectra obtained with the Bridge and Mushroom microdosimeter in response to 70 MeV ^{12}C ion at 90 µm depth in polyethylene. Two additional lines were added to mark the peaks being chosen for the LET_{MCA} calculation for Bridge and Mushroom microdosimeters.

Fig. 6a shows a comparison of LET and LET_{MCA} values in silicon for Lithium ions of different energies in silicon calculated using SRIM, Geant4 simulation and experiment using the Mushroom and Bridge microdosimeters. The experimental results for Lithium matched values from SRIM better at energies from 20 MeV to 50 MeV. The LET_{MCA} values calculated in the experiment were slightly higher than those values calculated using SRIM and Geant4 for Li ions with energies below 20 MeV. Lithium ions with energy below ~6 MeV will stop in the detectors (stoppers). Since the thickness of the microdosimeter (~10 µm) is used as a constant to calculate LET_{MCA} this leads the experimentally derived LET_{MCA} to decrease. The same was valid for LET_{MCA} simulated with Geant4 at energy lower than ~ 6 MeV because of the ions stopping in the SV. The horizontal error bars were calculated based on the energy spread of the ion when the thickness of the polyethylene absorbers varied between ± 2 µm from the nominal thickness. The uncertainty of LET (vertical error bars) was calculated based on the uncertainty in the thickness of the SOI active layer (±0.5 µm) and uncertainty of ion energies which is related to uncertainty of absorber's thicknesses included in the horizontal error bars.

Fig. 6b shows a comparison of LET values for Carbon ions of different energies in silicon calculated using SRIM, Geant4 simulation and experiment with the Mushroom and Bridge microdosimeters. It can be seen that when the ion energy is high, where ions do not stop in the detector, that the experimental LET_{MCA} values for both types of microdosimeters match the Geant4 simulation reasonably well within error bars. When the ion energy decreases from passing through the polyethylene absorbers, the experimental LET_{MCA} results are slightly higher than the simulated Geant4 and SRIM results. These discrepancies can be attributed to the uncertainty in the thickness of Polyethylene as well as the overlayers of the Bridge and Mushroom microdosimeter. Moreover, similarly to Li ions, low energy carbon ions below ~12 MeV will stop in 10 µm thick active layer of SOI microdosimeter after passing through the overlayers leading to a continuing decrease of the derived LET_{MCA}.

As we move to heavier ions, such as Oxygen and Titanium it can be seen that the discrepancy between the experimental and simulated results increases significantly. These discrepancies can be attributed to three main sources of uncertainty, uncertainty in absorber and overlayer thicknesses and non-uniform ionizing energy deposition in a SV when the range of the ion is approaching the thickness of the SV. The latter is contributing to increasing discrepancies between Geant4 simulated LET_{MCA} values and SRIM LET values for O ion energy below about 37 MeV and before reaching the maximum Geant4 LET_{MCA} value. The effect of the uncertainty in the overlayer thickness becomes amplified when the LET increases and more energy is lost in the overlayer, making the energy of the ion as it enters the SV less precisely known. Additionally, there have been very few studies measuring such low energy ions with silicon detectors which make comparisons difficult.

Fig. 6c shows a comparison of LET values for Oxygen ions of different energies in silicon calculated using SRIM, Geant4 simulation and experiment with the Mushroom and Bridge microdosimeter. It can be seen that at the higher ion energies that the experimental results for both types of microdosimeters match reasonably well with the Geant4 simulation. As the ion energy decreases, the LET_{MCA} measured by the microdosimeters becomes significantly higher than predicted by Geant4. For all the other ions, the Bridge microdosimeter consistently produces a higher LET_{MCA} value than the Mushroom microdosimeter, which is expected as the Bridge is thicker and has more overlayers than the Mushroom, and this is confirmed by stoppers being present for higher ion energy for the Bridge than the Mushroom. However, with Oxygen, the Mushroom microdosimeter derived higher LET values within the 20-60 MeV range, which can be attributed to less radiation damage within the Mushroom in comparison with the Bridge microdosimeter, as Oxygen irradiation was conducted after both Carbon and Lithium irradiation on the same devices (see radiation damage section below).

Fig. 6d shows a comparison of experimental and Geant4 LET_{MCA} values for Titanium ions of different energies in silicon with calculated values using SRIM for both microdosimeters. Due to the very short range and extremely high LET of Titanium ions, the uncertainty in absorber thickness and the overlayers of the devices lead to large discrepancies between the experimental and simulated results. Referring to Fig. 3a, it can be seen that the Bridge microdosimeter has much thicker and more complex overlayers in comparison to the Mushroom microdosimeter (Fig. 3b). Therefore, for higher energies Ti ions, the higher LET_{MCA} values measured by the Bridge, compared to Mushroom, are expected. Slightly reduced LET_{MCA} calculated by Geant4 in comparison with LET predicted by SRIM was observed for the ion energy higher than 75 MeV because the LET of Ti ions is reducing with fast degradation of Ti ion energy as ion traversing the SV in contrast to its increasing as in case of Li, C and O ions. This is due to much smoother and spread LET maximum (see SRIM LET curve, Fig 6d)) vs Ti ion energy in contrast to clear observed sharp maximum shifted to very low ion energy for Li, C and O ions.

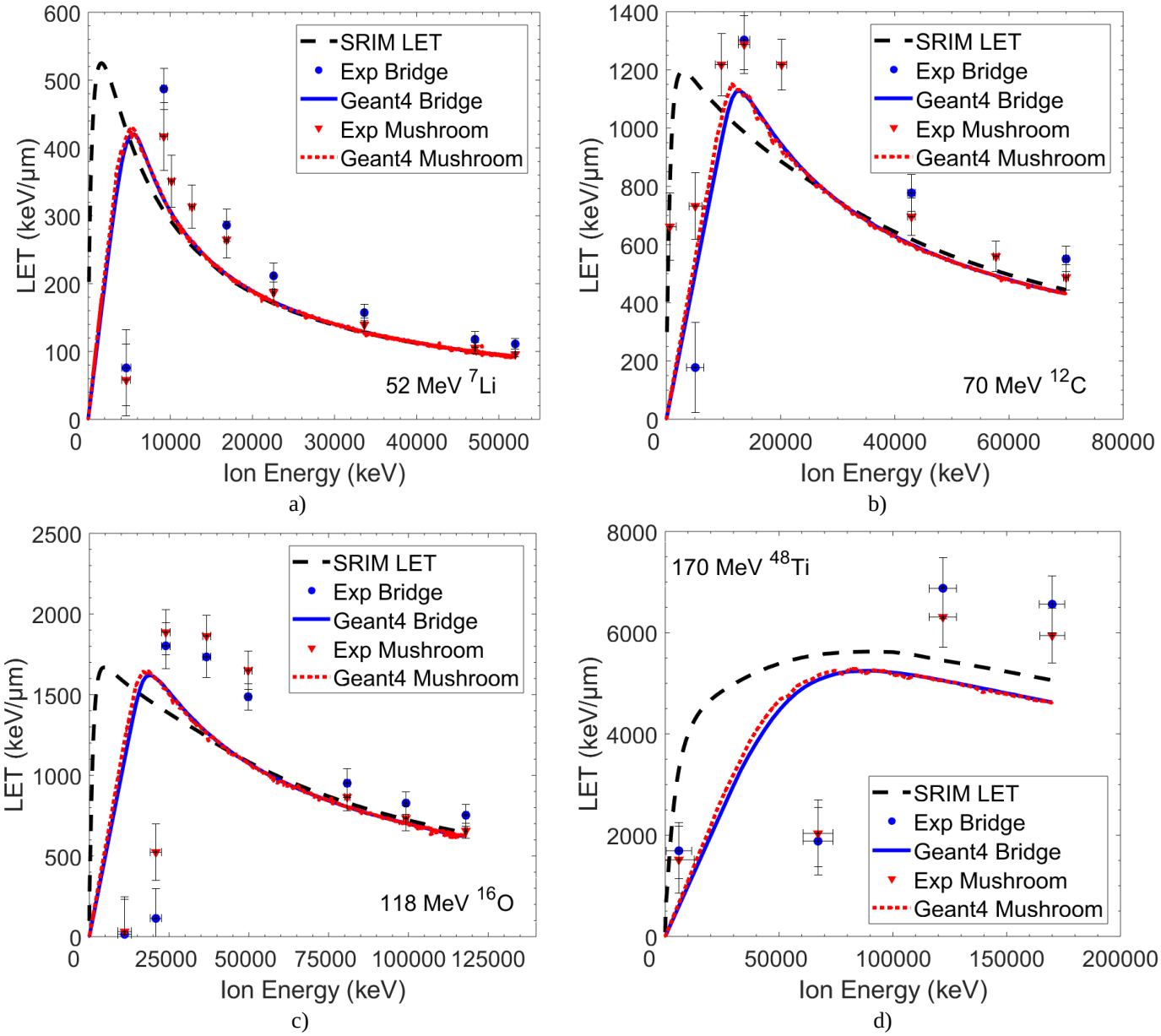

Fig. 6. LET_{MCA} measurements by SOI Bridge and Mushroom microdosimeters with different thicknesses of low density polyethylene (LDPE) for a) 52 MeV ^{7}Li, b)70 MeV ^{12}C, c) 118 MeV ^{16}O and d) 170 MeV ^{48}Ti ions in comparison with Geant4 simulation and SRIM data.

This also explains that for about 70 MeV Ti ions, why much lower derived experimental LET_{MCA} values were seen in comparison with Geant4. Experimentally, Ti ions enter the SV with lower energy than calculated by Geant4 due to thicker overlayers than assumed in Geant4 simulations. Experimental points for 10 MeV Ti ions are related to stoppers.

From these results the importance of having minimal overlayers, reducing both the thickness and complexity of these layers to minimize energy loss uncertainty can be seen. At higher ion energies these uncertainties are small, but rapidly increase with decreasing energy, and increasing LET, of the ions.

B. Microdosimetric Measurements of Oxygen Ions

Fig. 7 shows the dose mean lineal energy $\overline{y_D}$ distribution obtained with the Mushroom microdosimeter and Geant4 simulation as a function of depth in LDPE for the 118 MeV ^{16}O pristine BP. It can be seen that the experimental $\overline{y_D}$ values are slightly lower than the simulated $\overline{y_D}$. This is due to the fact that the simulation did not take into account the low energy events in the connecting region between the SVs of the Mushroom microdosimeter (see blue regions in Fig. 10a) [1].

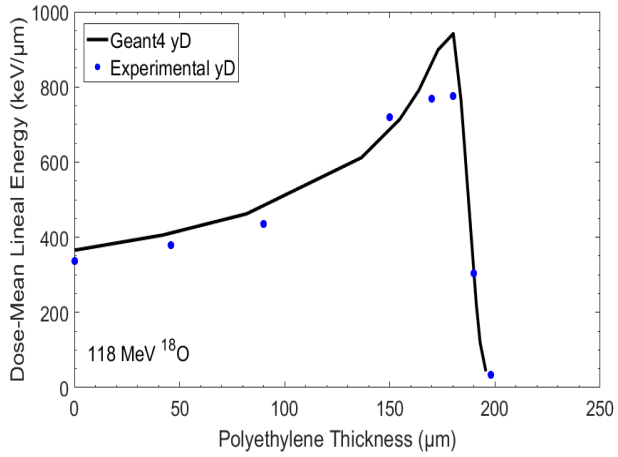

Fig. 7. Dose-mean lineal energy $\overline{y_D}$ distribution obtained with the Mushroom microdosimeters (dot) and Geant4 simulation (solid line) as a function of depth in LDPE for the 118 MeV ^{16}O pristine BP.

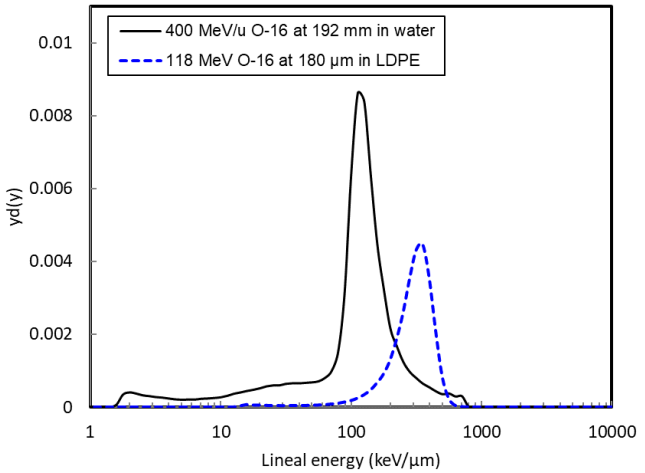

Fig. 8. Microdosimetric spectra measured using the Mushroom microdosimeter with 400 MeV/u ^{16}O ion pristine BP beam at 192 mm in water (solid line) and 118 MeV (7.375 MeV/u) ^{16}O ions at 180 µm LDPE film (dash line).

Fig. 8 shows the microdosimetric spectra obtained with the Mushroom microdosimeter at the distal edge of the BP of 400 MeV/u and 118 MeV (7.375 MeV/u) ^{16}O ions at HIMAC and ANU, respectively. In the case of the 400 MeV/u ^{16}O beam, the microdosimetric spectrum is more widely distributed over the lineal energy range. This broader distribution of the 400 MeV/u spectrum is due to the more pronounced secondary radiation field made up of many fragments and neutrons. While in the case of the 118 MeV ^{16}O ions, the microdosimetric spectrum was produced predominantly by oxygen ions only, with negligible contribution from fragmentation and neutrons due to low energy of the ions while ending point of both spectra are the same. Another reason for the broader 400 MeV/u spectrum is due to the much more pronounced straggling in the range. From the pinnacle of the BP in water to the distal 50% value of the pinnacle is more than 1 mm for the 400 MeV/u beam while the total range of the 7.375 MeV/u beam is only ~0.2 mm.

C. Radiation Damage

After irradiation with various energies of Li and Ti ions at ANU as well as irradiating the device in an IBIC study, it has been observed that the leakage current on the Mushroom microdosimeter substantially increased from 6 nA to 15 nA before and after irradiation, respectively. The Bridge microdosimeter was tested with IBIC and was irradiated with Ti ions only and shows a leakage current increase from 0.8 nA compared to 1.6 nA, before and after, respectively.

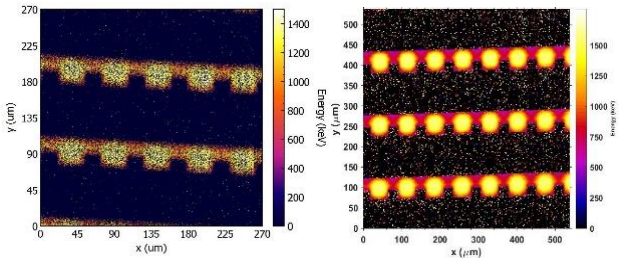

(a) (b)

Fig. 9. Median energy maps of charge collection in the Bridge microdosimeter at 10 V a) before and b) after irradiation with Ti ions

Fig. 9 shows median energy maps (IBIC study) obtained with the Bridge microdosimeter before and after irradiation with Ti ions with an integral fluence of about 1x10^8 cm^{-2}. No visible effect of CCE degradation was seen in the Bridge microdosimeter. Fig. 10 shows median energy maps obtained with the Mushroom microdosimeter before and after irradiation. It can be seen that after irradiation, low energy events corresponding to uniform charge collection outside of the SVs are present. This can be explained due to sufficient creation of the buildup charge in the oxide layer over the surface of the microdosimeter by low energy ions (Fig. 10b).

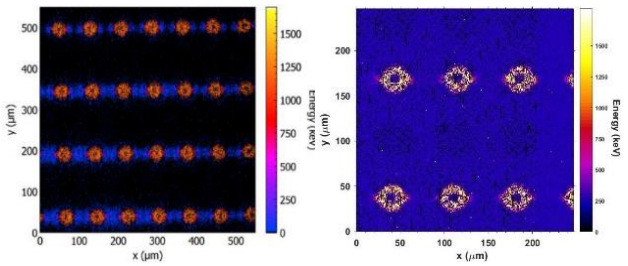

(a) (b)

Fig. 10. Median energy maps of charge collection in the Mushroom microdosimeter at 10 V a) before and b) after irradiation with Li, Ti ions.

Charge buildup in the SiO_2 layer produces an inverse layer under the silicon oxide in silicon and a depletion region approximately 1 µm thick, which leads to partial deposition

of ion energy and can be seen as low energy events uniformly distributed on the surface of the device. To overcome this, future versions of the Mushroom microdosimeter will be etched out entirely, like the Bridge microdosimeter, to avoid low energy events. However, no significant damage causing the reduction of charge collection efficiency in the SVs was observed in both devices when biased at 10 V. While in both detectors relative leakage current almost doubled, the Mushroom detector was irradiated with both Ti and Li ions with an integral fluence of about $5x10^8$ cm^{-2}, 5 times more than the Bridge microdosimeter.

Following the measurements at ANU a new generation of the Mushroom silicon microdosimeter has been fabricated and is entirely etched outside of the SVs. The new version of the Mushroom has been investigated using the IBIC technique with 5.5 MeV He^{2+} ions revealing no low energy events from the passive silicon region connecting the SVs. Each of the sensitive volumes has very uniform charge collection, in addition to excellent sensitive volume definition, without cross talk between the adjacent sensitive volumes as seen in Fig. 11:

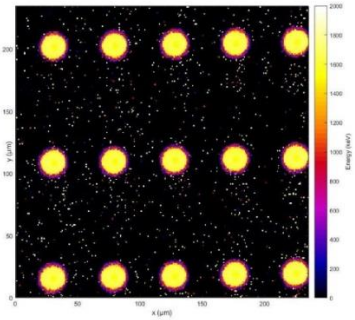

Fig. 11. Median energy map of charge collection within the new fully etched generation Mushroom microdosimeter at 10V bias.

IV. Conclusion

The responses of 3D silicon microdosimeters developed by CMRP were investigated with low energy ions. It has been shown that for Li, C and O ions, the experimental results matched better with SRIM and Geant4 simulation at higher ion energies. The discrepancies are amplified with greater thicknesses of polyethylene which cause increased straggling of the ions, as well as increasing the uncertainty in the absorber thickness. The complexity of overlayers on the microdosimeters plays an important role in the accuracy of the LET measurements for low energy ions due to uncertainty in energy loss. It has been demonstrated that no plasma effect was seen in both SOI microdosimeters when irradiating with such high LET ions. The Mushroom microdosimeter has a stronger electric field in SV in comparison with the Bridge microdosimeter, however build up charge effects within the SiO_2 has caused low energy events to be shared between the SVs of the mushroom microdosimeter. This problem has been addressed in the newer design of the mushroom microdosimeter.

To achieve more accurate LET measurements, devices with thinner, more simplistic overlayers should be adopted, something which is not always possible with the current level of industrial technology while keeping reliable passivation of SVs for field operation of the device. Future work should be dedicated to fabrication of 3D SOI microdosimeters, which are fully etched and have simpler and thinner overlayers than current designs and fabricated on a thinner SOI active layer to utilize them for more accurate microdosimetry of ions with low energies.

Acknowledgement

This research was supported by the Australian Government through the Australian Research Council's Discovery Projects funding scheme (projects DP 170102273 and DP170102423). Operation of the ANU Heavy Ion Accelerator Facility is supported by NCRIS. The authors acknowledge Dr. Andrew See and his team at the UNSW ANFF node for their packaging work. Finally, the authors thank all collaborators in the 3D-MiMiC project, funded by the Norwegian Research Council via the NANO2021 program.

References

[1] A. B. Rosenfeld, “Novel detectors for silicon based microdosimetry, their concepts and applications,” Nucl. Instrum. Meth., Phys. Res. A, vol. 809, pp. 156–170, February 2016.

[2] T. Inaniwa, “Treatment planning of intensity modulated composite particle therapy with dose and linear energy transfer optimization,” Phys. Med. Biol, Vol. 62, No. 12, Mar 2017.

[3] L. T. Tran, L. Chartier, D. Bolst, et al., “Thin silicon microdosimeter utilizing 3D MEMS technology: Charge collection study and its application in mixed radiation fields,” IEEE Transactions on Nuclear Science, vol. 65, no. 1, pp. 467–472, Oct 2017.

[4] L. T. Tran, L. Chartier, D. Bolst, et al., “3D silicon microdosimetry and rbe study using ^{12}C ion of different energies,” IEEE Transactions on Nuclear Science, vol. 62, no. 6, pp. 3027–3033, Dec 2015.

[5] J. F. Ziegler, M. D. Ziegler, J. P. Biersack, et al, “SRIM - The stopping and range of ions in matter,” Nucl. Instrum.Methods Phys. Res. B., vol. 268, no. 11–12, pp. 1818–1823, Jun. 2010.

[6] M. J. Berger, J. S. Coursey, M. A. Zucker and J. Chang, “ESTAR, PSTAR, and ASTAR: Computer Programs for Calculating Stopping-Power and Range Tables for Electrons, Protons, and Helium Ions (version 2.0.1)”, July. 2017, Available: http://physics.nist.gov/Star [2018, July 8th]. National Institute of Standards and Technology, Gaithersburg, MD.

[7] S. Agostinelli, J. Allison, K. Amako, et al., “Geant4a simulation toolkit,” Nuclear Instruments and Methods in Physics Research Section A: Accelerators, Spectrometers, Detectors and Associated Equipment, vol. 506, no. 3, pp. 250 – 303, July 2003.

[8] J. Allison, K. Amako, J. Apostolakis, et al., “Geant4 developments and applications,” IEEE Transactions on Nuclear Science, vol. 53, pp. 270–278, Feb 2006.

[9] S. Chauvie, Z. Francis, S. Guatelli, et al., “Geant4 physics processes for microdosimetry simulation: Design foundation and implementation of the first set of models,” IEEE Transactions on Nuclear Science, vol. 54, pp. 2619–2628, Dec 2007.

[10] K. Amako, S. Guatelli, V. N. Ivanchenko, et al., “Comparison of geant4 electromagnetic physics models against the nist reference data,” IEEE Transactions on Nuclear Science, vol. 52, pp. 910–918, Aug 2005.

[11] Z. Pastuovic, R. Siegele, D. Cohen, et al., “The new confocal heavy ion microprobe beamline at ANSTO,” Nuclear Instruments and Methods in Physics Research Section B: Beam Interactions with Materials and Atoms, vol. 404, pp. 1 – 8, Aug 2017.